Experimental study of isospin transport with ^{40,48}Ca + ^{40,48}Ca reactions at 35 MeV/nucleon

Q. Fable [1,*], A. Chbihi,[2] J. D. Frankland,[2] P. Napolitani,[3] G. Verde,[1,4] E. Bonnet,[5] B. Borderie,[3] R. Bougault,[6] E. Galichet,[3,7] T. Génard,[2] D. Gruyer,[6] M. Henri,[2] M. La Commara,[8] A. Le Fèvre,[9] J. Lemarié,[2] N. Le Neindre,[6] O. Lopez,[6] P. Marini,[10] M. Pârlog,[6,11] A. Rebillard-Soulié,[6] W. Trautmann,[9] E. Vient,[6] and M. Vigilante[12,13]

(INDRA Collaboration)

[1]*Laboratoire des 2 Infinis - Toulouse (L2IT-IN2P3), Université de Toulouse, CNRS, UPS, F-31062 Toulouse Cedex 9, France*
[2]*GANIL, CEA/DRF-CNRS/IN2P3, Boulevard Henri Becquerel, F-14076 Caen Cedex, France*
[3]*Université Paris-Saclay, CNRS/IN2P3, IJCLab, 91405 Orsay, France*
[4]*Istituto Nazionale di Fisica Nucleare, Sezione di Catania, 64 Via Santa Sofia, I-95123 Catania, Italy*
[5]*SUBATECH UMR 6457, IMT Atlantique, Université de Nantes, CNRS-IN2P3, 44300 Nantes, France*
[6]*Normandie Univ, ENSICAEN, UNICAEN, CNRS/IN2P3, LPC Caen, F-14000 Caen, France*
[7]*Conservatoire National des Arts et Métiers, F-75141 Paris Cedex 03, France*
[8]*Dipartimento di Farmacia, Università Federico II and INFN Napoli, Napoli, Italia*
[9]*GSI Helmholtzzentrum für Schwerionenforschung GmbH, D-64291 Darmstadt, Germany*
[10]*Univ. Bordeaux, CNRS, LP2I, UMR 5797, F-33170 Gradignan, France*
[11]*National Institute for Physics and Nuclear Engineering, RO-077125 Bucharest-Măgurele, Romania*
[12]*Dipartimento di Fisica, Università degli Studi di Napoli FEDERICO II, I-80126 Napoli, Italy*
[13]*Istituto Nazionale di Fisica Nucleare, Sezione di Napoli, Complesso Universitario di Monte S. Angelo, Via Cintia Edificio 6, I-80126 Napoli, Italy*

We investigate the isospin transport with ^{40,48}Ca + ^{40,48}Ca reactions at 35 MeV/nucleon, measured with the coupling of the VAMOS high acceptance spectrometer and the INDRA charged particle multidetector. Using the fragment measured with VAMOS and carefully selected light-charged-particles measured in coincidence with INDRA, a reconstruction method is applied to estimate the excited quasiprojectile (QP) on an event-by-event basis. Isospin diffusion is investigated using the isospin transport ratio with the asymmetry $\delta = (N - Z)/A$ of the projectile remnant as an isospin-sensitive observable and the total transverse energy of $Z \leqslant 2$ nuclei for experimental centrality sorting. The experimental isospin transport ratios present, for both the reconstructed QP and its remnant, a clear evolution towards isospin equilibrium with increasing dissipation of the collision while the full equilibration is not reached. A smoother evolution with less discrepancies between the two mixed systems in the case of the reconstructed QP is also observed. Isospin migration is investigated using the average neutron-to-proton ratio of the light-charged-clusters and the velocity of the QP remnant as a sorting parameter. A systematic neutron-enrichment is observed and interpreted as a consequence of isospin migration, in particular for the symmetric systems which present no isospin gradient between the projectile and the target. We also noticed that the ^{2}H and ^{4}He particles exhibit very close multiplicities independently of the sorting variable for the symmetric systems.

DOI: 10.1103/PhysRevC.107.014604

I. INTRODUCTION

The equation of state (NEoS) of bulk nuclear matter over a wide range of densities, temperatures and neutron-to-proton asymmetries remains a major issue in modern nuclear physics and astrophysics. Indeed, the NEoS plays a key role in describing nuclear systems probed in laboratory experiments, as well as in modeling neutron stars, core-collapse supernovae (CCSN) and mergers of compact binary stars [1]. Heavy-ion collisions (HIC) are the unique tool to probe the NEoS at finite temperature under laboratory controlled conditions, over

a wide range of density and energy, depending on the beam energy, the size of the colliding systems and the impact parameter of the collisions. Such experiments allow one to constrain the isoscalar (same proton, ρ_p, and neutron, ρ_n, densities) and isovector ($\rho_p \neq \rho_n$) contributions to the energy density of nuclear matter away from saturation density, $\rho_0 \simeq 0.17$ fm^{-3} [2]. At intermediate beam energies (20–100 MeV/nucleon), temperatures and densities similar to those reached in the neutrinosphere of CCSN matter are expected, allowing the experimental study of in-medium effects of light clusters at high temperature [3]. At higher beam energies, NEoS constraints for symmetric nuclear matter [4] and symmetry energy [5] are probed at densities in the range of roughly ρ_0-to-3ρ_0 and ρ_0-to-2ρ_0, respectively. In particular, a recent

interdisciplinary analysis from Huth *et al.* demonstrated the benefit of combining astrophysical multimessenger observations from gravitational-wave astronomy [6] and electromagnetic observations of neutron stars [7] with HIC results to provide complementary information on the NEoS at intermediate densities [8].

As the NEoS cannot be measured directly, it can only be inferred from comparisons of model predictions with carefully selected collision observables. For example, transport models are used to predict the dynamics of HIC by numerically solving equations based on semiclassical mean-field approximations, including correlations via nucleon-nucleon collisions and a given parametrization of the NEoS via effective interactions. Peripheral and semiperipheral reactions around Fermi energy (30–60 MeV/nucleon) are of particular interest to study the transport of nuclear matter and N/Z equilibration effects. Indeed such reactions are dominated by binary-like collisions, where projectile and target nuclei interact by exchanging nucleons before reseparating into a quasiprojectile (QP) and a quasitarget (QT), with kinematic properties respectively close to the projectile and the target, but also by the production of lighter ejectiles like light-charged particles (LCPs, $Z = 1, 2$) and intermediate-mass fragments (IMFs, $3 \leqslant Z \leqslant 6$ in the present work) [9–11]. As QP and QT can be moderately deformed and excited, they are expected to undergo sequential decays by emitting LCPs and gamma rays, leading to a projectile-like (PLF) and a target-like (TLF) fragment as remnants.

If the initial neutron-to-proton ratios N/Z of the reaction partners are different, isospin equilibration is expected to occur which will be reflected in the N/Z of the outgoing nuclei. This phenomenon, called isospin diffusion, is driven by the isospin gradient between the two colliding participants, which is proportional to the symmetry energy term of the NEoS. In addition, various transport model calculations suggest a neutron enrichment of the neck region developing between the QP and the QT and characterized by subsaturation densities ($\rho < \rho_0$) [2,12–17]. This phenomenon, called isospin migration (or drift), is driven by the density gradient between this neck region and the QP-QT remnants, which is proportional to the derivative of the symmetry energy term: a larger neutron enrichment of the neck is expected for a stiffer symmetry energy [17]. One can thus expect the degree of charge and mass equilibration occurring during the collision mainly to depend on the strength of the symmetry energy and the interaction time between the two reaction participants. Exploiting large-angular-acceptance detector arrays with different projectile and target combinations, it is possible to study the competition between isospin diffusion and migration while characterizing the dissipation of the collision. Of course, the timescales for each collision cannot be measured experimentally but only be inferred from measured final state observables. To draw conclusions, it is also necessary to consider the role of evaporation and promptly emitted particles that possibly modify the experimental observables.

This work presents the experimental investigation of the isospin transport in ^{40,48}Ca + ^{48,40}Ca reactions at 35 MeV/nucleon measured with the coupled INDRA-

TABLE I. Characteristics of the studied systems with E_{inc}, $B\rho_0$, and v_{lab} (respectively the beam incident energy, magnetic rigidity, and velocity in the laboratory frame), θ_{gr} the grazing angle, and I_{sys} the initial neutron-to-proton ratio of the total system.

Beam	E_{inc} (MeV/nuc)	$B\rho_0$ (T m)	v_{lab} (cm/ns)	Target	I_{sys}	θ_{gr} (deg)
^{40}Ca^{18+}	34.81	1.904	7.978	^{40}Ca	1.0	2.35
^{40}Ca^{18+}	34.81	1.904	7.978	^{48}Ca	1.2	2.29
^{48}Ca^{20+}	34.83	2.061	7.980	^{40}Ca	1.2	1.91
^{48}Ca^{20+}	34.83	2.061	7.980	^{48}Ca	1.4	1.86

VAMOS detectors and follows our previous study reported in [18] where a method to reconstruct the primary QP fragments was presented. Event by event, the PLF detected and identified by VAMOS was associated with coincident LCP detected in INDRA, taking care to exclude preequilibrium and neck emissions by exploiting velocity correlations of the LCPs with both PLF and TLF. As evaporated neutrons were not measured, mean neutron multiplicities extracted from AMD followed by GEMINI ++ calculations were used instead. More details can be found in [18].

The experimental setup is described in Sec. II. Section III presents the results on isospin diffusion and isospin migration, along with a comparison between the PLF measured in VA-MOS and the reconstructed QP. A summary and conclusions are finally presented in Sec. IV.

II. EXPERIMENTAL SETUP

The experiment was performed at the GANIL facility, where beams of ^{40,48}Ca at 35 MeV/nucleon impinged on self-supporting 1.0 mg/cm^2 ^{40}Ca or 1.5 mg/cm^2 ^{48}Ca targets placed inside the INDRA vacuum chamber. The typical beam intensity was around 5.10^7 pps. The detection system consisted of the coupling of the 4π charged particle array INDRA [19,20] and the VAMOS spectrometer [21]. Table I gives a summary of the characteristics of the studied systems.

Concerning the charged particle multidetector array IN-DRA, the detection telescopes are arranged in rings centered around the beam axis. In this experiment, INDRA covered polar angles from 7° to 176°. Rings 1 to 3 were removed to allow the mechanical coupling with VAMOS in the forward direction. Rings 4 to 9 (7°–45°) consisted each of 24 three-layer detection telescopes: a gas-ionization chamber operated with C_3F_8 gas at low pressure, a 300 or 150 μm silicon wafer, and a CsI(Tl) scintillator (14 to 10 cm thick) read by a photomultiplier tube. Rings 10 to 17 (45°–176°) included 24, 16, or 8 two-layer telescopes: a gas-ionization chamber and a CsI(Tl) scintillator of 8, 6, or 5 cm thickness. Fragment identification thresholds are about 0.5 and 1.5 MeV per nucleon for the lightest ($Z \lesssim 10$) and the heaviest fragments, respectively. INDRA allows charge and isotope identification up to Be-B and only charge identification for heavier fragments. A detailed description of the INDRA detector and its electronics can be found in [19,20].

The VAMOS spectrometer is composed of two large magnetic quadrupoles focusing the incoming ions in the vertical
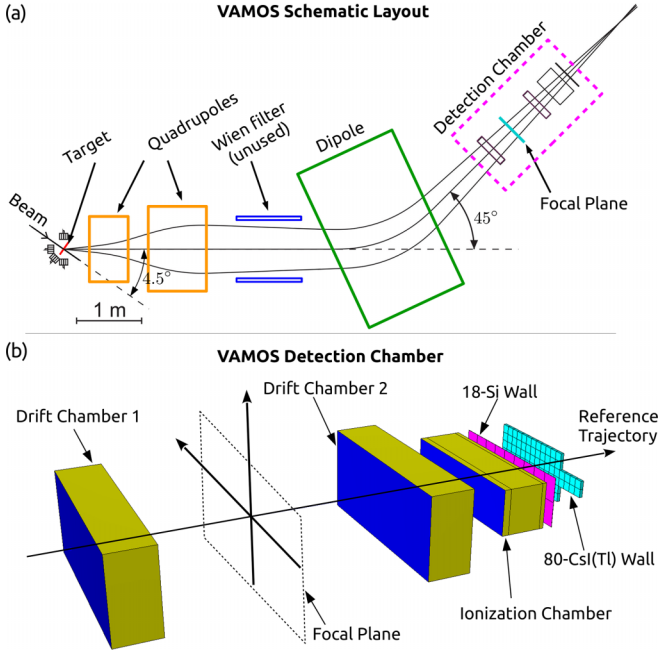
FIG. 1. (a) VAMOS schematic layout. The spectrometer was rotated at 4.5° with respect to the beam axis for the present experiment. (b) Global three-dimensional view of the VAMOS detection chamber. The reference frame corresponds to the reference trajectory. Adapted from [21].

and horizontal planes and a large magnetic dipole, which bends the trajectory of the ions.

A representation of the VAMOS optical line is given in Fig. 1(a). In the present setup, the spectrometer was rotated at 4.5° with respect to the beam axis, so as to cover the forward polar angles from 2.56° to 6.50°, thus favoring the detection of a fragment emitted slightly above the grazing angles of the studied reactions. The momentum acceptance was about ±5%, and the focal plane was located 9 m downstream, giving a large enough time of flight (ToF) base to allow a mass resolution of about $\Delta A/A \approx 1/165$ for the isotopes produced in the collisions.

A three-dimensional view of the spectrometer detection chamber, located upstream and downstream of the focal plane (FP), is presented in Fig. 1(b). The VAMOS detection setup of the experiment included two position-sensitive drift chambers used to determine the trajectories of the reaction products at the focal plane, followed by a sandwich of detectors: a seven-module ionization chamber, a 500 μm thick Si wall (18 independent modules), and a 1 cm thick CsI(Tl) wall (80 independent modules), allowing the measurements of the ToF, energy loss (ΔE), and energy (E) parameters. Around 12 magnetic rigidity ($B\rho_0$) settings, from 0.661 to 2.220 T m, were used for each system to cover the full velocity range of the fragments.

A description of the identification, reconstruction and event normalization procedures are given in [18].

At least one hit on the VAMOS silicon wall was required for each event to be acquired. Other trigger configurations, allowing one to select more central collisions, were also set

but will not be discussed in the present work. It should be noted that only multiplicity "1" events in the VAMOS Si wall are considered. This offline selection was applied to make sure that the positions measured in the drift chambers are correct and to avoid events with ambiguous trajectory reconstruction. The elastic-like events (corresponding to events with no hit in INDRA and a fragment identical to the projectile in VAMOS) were also removed offline.

III. ISOSPIN TRANSPORT

The stochastic, differential exchange of nucleons between two colliding nuclei with different N/Z, usually referred to as isospin transport, is expected to depend mainly on the difference in composition of the two nuclei, the interaction time of the collision, and the symmetry energy term of the NEoS. In a hydrodynamic approximation, the isospin transport can be described by means of the local neutron and proton currents $\mathbf{j}_n$ and $\mathbf{j}_p$, as [10,17]

$$\mathbf{j}_{n,p} = D_{n,p}^\rho \nabla\rho - D_{n,p}^\delta \nabla\delta, \tag{1}$$

where $\rho = \rho_n + \rho_p$ is the local density of nuclear matter, $\delta = (\rho_n - \rho_p)/\rho$ the neutron-to-proton asymmetry (isospin), and $D_{n,p}^{\rho,\delta}$ are the density and isospin-dependent transport coefficients for neutrons and protons [10].

According to Eq. (1),

$$\mathbf{j}_n - \mathbf{j}_p = \underbrace{\left(D_n^\rho - D_p^\rho\right)\nabla\rho}_{\text{isospin migration}} - \underbrace{\left(D_n^\delta - D_p^\delta\right)\nabla\delta}_{\text{isospin diffusion}}. \tag{2}$$

The first term of Eq. (2), called isospin migration (or isospin drift) can be related to the density dependence of the symmetry energy as

$$D_n^\rho - D_p^\rho \propto 4\delta \frac{\partial\epsilon_{\text{sym}}}{\partial\rho}. \tag{3}$$

The second term of Eq. (2), called isospin diffusion can be related to the value of the symmetry energy (at a given local density) as

$$D_n^\delta - D_p^\delta \propto 4\rho\epsilon_{\text{sym}} \tag{4}$$

During a collision, a rearrangement of the neutron-to-proton ratio of the colliding nuclei is expected to take place under the combined effect of (i) isospin migration (drift) leading to an increase in neutron richness of low-density regions and (ii) isospin diffusion leading to a balance in neutron richness of different isospin (δ) regions. Equations (3) and (4) hence suggest that one can use the measurements of N/Z-sensitive observables to probe the derivative and strength of ϵ_{sym}, respectively.

A. Isospin diffusion

Quantitative signals of the isospin diffusion phenomenon can be deduced from the isospin transport ratio (also known as imbalance ratio) introduced by Rami *et al.* [22]. This technique is based on combining isospin-sensitive observables measured with four systems differing in their initial neutron-to-proton ratio. Two symmetric neutron-rich (NR) and neutron-deficient (ND) reactions are used as reference

values, while the two mixed reactions (M) reach a neutron content in between these two references.

The isospin transport ratio is defined as

$$R_x = \frac{2x^M - x^{NR} - x^{ND}}{x^{NR} - x^{ND}}, \tag{5}$$

where x is an isospin-sensitive observable expected to be univocally related to the N/Z of the systems under study.

In order to follow the evolution of the system towards the N/Z equilibration, the R_x ratio is studied as a function of an ordering parameter directly related to the dissipation. By construction, $R_x = \pm 1$ in the limit of fully nonequilibrated conditions (isospin transparency). Moreover, $R_x = 0$ represents full isospin equilibration conditions of a mixed reaction if x presents a linear dependence on the isospin, whereas more generally equilibration is signalled by both mixed reactions achieving the same value for the ratio [22].

In particular, under identical experimental conditions, this ratio is expected to reduce the sensitivity to dynamical (fast emissions, Coulomb) and sequential decay effects while the associated errors remain statistical. According to the original work of Rami, R_x is expected to bypass any perturbation introducing a linear transformation of x. The validity of this assumption was recently studied in the framework of the Antisymmetrized Molecular Dynamics (AMD) transport model [23] coupled to different statistical decay codes [24]. A conclusion of that work was that the statistical deexcitation of the QP introduces a linear transformation of the N/Z of the projectile for an excitation energy $E^*/A \gtrsim 2$ MeV/nucleon, while a nonlinearity develops at lower excitation energies.

We also address this issue in the next sections with a comparison of the isospin transport ratio obtained from the PLF directly measured in VAMOS and the reconstructed QPs with the evaporated neutron estimation.

1. Estimation of experimental centrality

In the present study we will use the total transverse energy of LCPs, E_{t12}, as a measure of the violence of the collisions in order to estimate their centrality. E_{t12} is defined as

$$E_{t12} = \sum_{i:Z_i \leqslant 2} E_i \sin^2 \theta_i, \tag{6}$$

where in the sum i runs over the detected products of each event with $Z_i \leqslant 2$, laboratory kinetic energy E_i, and laboratory polar angle θ_i. This global variable has often been used in previous analyses, as it is particularly well-suited to the performances of the INDRA array for which LCPs are detected with a close-to-geometrical (90%) efficiency [25–28]. In the context of the present analysis it is also worth noting that the PLF properties are completely independent of this quantity, avoiding possible trivial bias due to autocorrelation with the event sorting for the study of the isospin transport ratio presented in Sec. III A 3.

The inclusive E_{t12} distributions for the four systems under study are shown in Fig. 2. The distributions are presented with a logarithmic y-axis scale in order to emphasize the differences in the high-E_{t12} tails, which to a first approximation can be associated with the most central collisions. We observe that
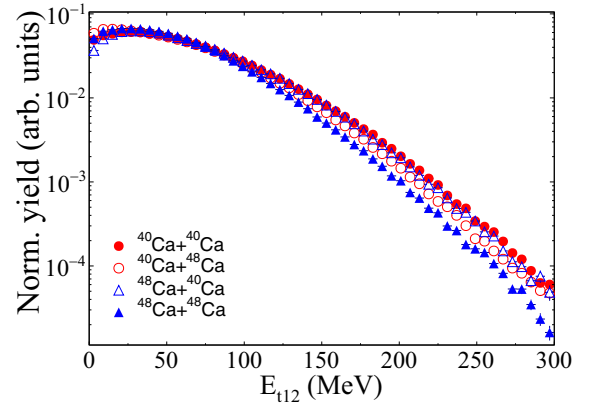

FIG. 2. Total transverse energy distributions of light charged particles (normalized to their integral) for ^{40,48}Ca $+ ^{40,48}$Ca collisions at 35 MeV/nucleon. Statistical errors are represented by vertical bars when larger than the symbols.

for the system ^{40}Ca $+ ^{40}$Ca higher E_{t12} values are explored in the tail compared to the neutron-rich ^{48}Ca $+ ^{48}$Ca one, while the two "crossed" systems, ^{40}Ca $+ ^{48}$Ca and ^{48}Ca $+ ^{40}$Ca, reach intermediate values. This means that E_{t12} values for the different systems are not directly comparable, and data for the different systems with similar E_{t12} values cannot be assumed to have similar centrality.

In order to remove the trivial system-dependence of the E_{t12} distributions, $P(E_{t12})$, we will sort data according to the experimental centrality, $c_{E_{t12}}$, defined as

$$c_{E_{t12}} \equiv \int_{E_{t12}}^{+\infty} P(\tilde{E}_{t12}) \, d\tilde{E}_{t12} \tag{7}$$

which is nothing but the complementary cumulative distribution function or tail function of the distribution $P(E_{t12})$. By construction, $c_{E_{t12}}$ decreases from 1 to 0 as E_{t12} goes from its minimum ($\approx$0) to its (system-dependent) maximum value, therefore in the following we will associate large ($\approx$1) $c_{E_{t12}}$ values with the most peripheral collisions recorded for each system, while smaller values ($c_{E_{t12}} \to 0$) indicate increasing centrality *i.e.* smaller average impact parameters. It should be noted that a further advantage of sorting according to centrality as defined in Eq. (7) is that $c_{E_{t12}}$ bins of fixed width contain the same number of events or fraction of the total recorded cross-section, and therefore have the same statistical significance, whatever the centrality.

2. N/Z asymmetry of the projectile

In this section we present the general features of the experimental observable used to compute the isospin transport ratio from Eq. (5).

The asymmetry $\delta = (N - Z)/A$ of the PLF or the QP was chosen as an isospin sensitive observable as it has proved to be a suitable tool for investigating the stiffness of the NEoS [17,29]. It should be noted that the results and conclusions presented hereafter can also be drawn using the neutron-to-proton ratio N/Z.
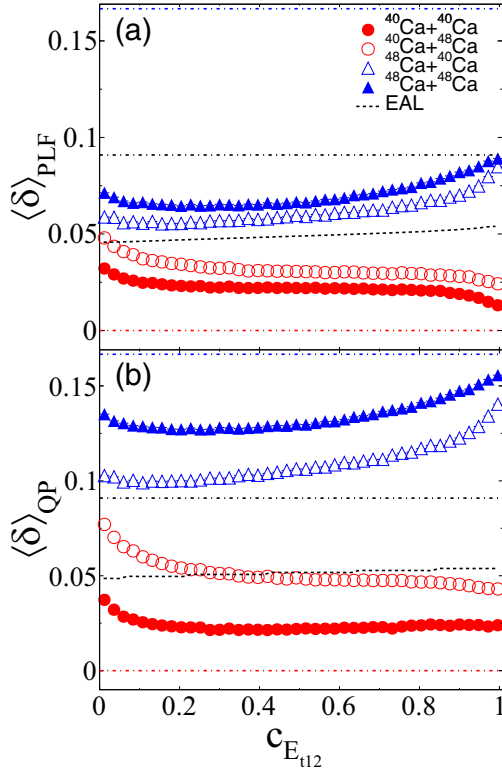
FIG. 3. Distribution of the average asymmetry δ as a function of the experimental centrality $c_{E_{t12}}$ for (a) the PLF and (b) the reconstructed QP for the four systems under study. Statistical error bars are smaller than the symbols. The initial asymmetries of the colliding systems and the EAL extracted from [30] (using the average charge of the symmetric systems for each bin of $c_{E_{t12}}$) are represented by dotted-dashed and dashed lines, respectively.

Figure 3 presents the evolution of the average asymmetry of the PLF and of the reconstructed QP as a function of the experimental centrality $c_{E_{t12}}$. The PLF distributions, shown in Fig. 3(a), exhibit an ordering according to the neutron-richness of the projectile and to a lesser extent of the target, similarly to the charge distributions reported in our previous work [18]. In addition, we observe an increase (respectively a decrease) of the asymmetry with increasing $c_{E_{t12}}$ for the ^{48}Ca (respectively ^{40}Ca) projectile reactions. We also notice that the initial asymmetries ($\delta_{4040} = 0$, $\delta_{4048} = \delta_{4840} = 0.091$, and $\delta_{4848} = 0.167$, represented with dotted-dashed lines) of the colliding nuclei is not reached, even for the less central collisions ($c_{E_{t12}} \simeq 1$). It is worth noting that for the most peripheral collisions a mean neutron excess of 4 ($\delta = 0.091 = \delta_{4840}$) is measured for Ca isotopes with ^{48}Ca projectile reactions, while a mean neutron deficit of 1 is obtained for the ^{40}Ca projectile. The average loss of four neutrons for neutron-rich projectile systems can be prevalently associated with neutron evaporation from the excited projectile residue. An additional contribution from neutron transfer should result in an enhanced shift of the isotopic content towards the residue corridor for the asymmetric systems. Less neutron rich than the β-stability line, the residue corridor, or evaporation attractor line (EAL, represented here in dashed lines for the

symmetric systems and extracted from [30]), is a region of the nuclear chart where proton and neutron emissions have equal probability. It is reached when enough excitation energy feeds the decay, rather than other more violent decay mechanisms. For the ^{48}Ca projectiles, this effect even counterbalances the fact that the asymmetric system should correspond to less excitation energy available for the secondary decay (due to the smaller target) so that, in the absence of diffusion and relying on a simple sequential-decay picture, the residues produced with the ^{48}Ca $+$ ^{48}Ca system should approach the EAL more closely than the ^{48}Ca $+$ ^{40}Ca system. The opposite is observed in the present case, likely due to isospin diffusion contributions. For the ^{40}Ca projectiles, the two effects should, on the other hand, act in phase. It is interesting that the opposite effect was observed at relativistic energies in [31,32], where a prevalent contribution from multifragmentation was taking excitation away from the secondary decay process, preventing the system from reaching the EAL. A quantitative description of the distributions of Fig. 3(a) should also involve the emission of light clusters, in particular for the ^{40}Ca projectile systems and the side related to larger centrality, as more excitation energy would feed cluster emission.

Concerning the reconstructed QP asymmetry presented in Fig. 3(b), the same trend and hierarchy as for the PLF distributions are observed. As expected, the reconstructed δ are further away of the EAL than in the case of the PLF with higher gaps between the distributions. We remark that the ^{48}Ca projectile reactions present systematically higher values than the initial asymmetry of the asymmetric reactions ($\delta_{4048} = \delta_{4840} = 0.091$). with lower values than the neutron rich system ($\delta_{4848} = 0.167$). For the most peripheral collisions a mean neutron excess of 6 ($\delta = 0.130$) is measured for Ca isotopes with ^{48}Ca projectile reactions, while a mean neutron deficit of 0.5 is obtained for the ^{40}Ca projectile. Finally, it is worth noting that a tendency to reach the initial asymmetry with decreasing $c_{E_{t12}}$ (more central collisions) is observed for the asymmetric systems.

3. Isospin transport ratio

For each bin of experimental centrality $c_{E_{t12}}$, the isospin transport ratio R_δ was computed from Eq. (5) using the average asymmetry $\langle \delta \rangle = \langle (N - Z)/A \rangle$ as the isospin-sensitive observable, with ^{40}Ca $+$ ^{48}Ca or ^{48}Ca $+$ ^{40}Ca as mixed systems (M), ^{48}Ca $+$ ^{48}Ca as neutron-rich system (NR), and ^{40}Ca $+$ ^{40}Ca as neutron-deficient system (ND). The results are presented in Fig. 4 for the PLF (open symbols) and the reconstructed QP (full symbols). For both, an evolution of the isospin transport ratio is observed, with decreasing values from about $R_\delta = \pm 0.75$ to about $R_\delta = \pm 0.3$ when moving from the most peripheral collisions (high $c_{E_{t12}}$ values) to the most central collisions (low $c_{E_{t12}}$ values). Moreover the mean value of R_δ for the two crossed reactions, averaged over the $c_{E_{t12}} < 0.1$ region (corresponding to the most central collisions), is very small ($R_\delta = 0.04 \pm 0.05$ for the QP and $R_\delta = 0.04 \pm 0.07$ for the PLF, represented by a dashed line) thus demonstrates the linear dependence of δ [22]. The data thus suggest a continuous evolution towards an N/Z equilibration condition, while a full equilibration condition is not reached
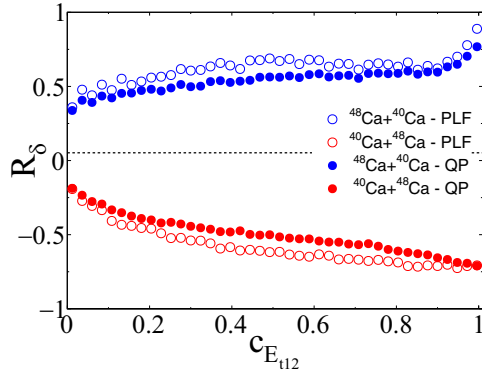
FIG. 4. Isospin transport ratios computed from the asymmetry δ of the QP remnant (open symbols) and the reconstructed QP (full symbols) as a function of the experimental centrality $c_{E_{t12}}$. Statistical error bars are smaller than the symbols. The dashed line corresponds to the mean value ($R_\delta = 0.04$) of the ^{40}Ca + ^{48}Ca and ^{48}Ca + ^{40}Ca experimental points in the $c_{E_{t12}} \leqslant 0.1$ region.

even in the most central collisions. It is worth noting that indirect indications, obtained from mirror nuclei yield ratios, of such an evolution of the isospin transport ratio with centrality were already reported in [33]. However, the results reported in the present article are a direct estimate of the N/Z of both the PLF and the QP performed with the coupled INDRA-VAMOS device.

It should be also highlighted that the reconstructed QP presents a smoother evolution, with less disparities and a slower evolution to the full equilibration, compared to the case of the PLF. As demonstrated in [29,34], for a given sorting parameter, the experimental isospin transport ratio can present variations in its absolute values depending on the isospin-sensitive probe, while the trend towards isospin equilibration was nonetheless observed.

In order to study the effect of the QP reconstruction on the experimental isospin transport ratio, we present in Fig. 5 the average PLF asymmetry, $\langle\delta\rangle_{PLF}$, as a function of the QP asymmetry, δ_{QP}, for three ranges of $c_{E_{t12}}$ values, namely $0.05 < c_{E_{t12}} < 0.1$ (central collisions, left panel), $0.45 < c_{E_{t12}} < 0.5$ (mid-central collisions, central panel), and $0.85 < c_{E_{t12}} < 0.9$ (peripheral collisions, right panel). In particular, $\langle\delta\rangle_{PLF}$ was

computed for each bin of δ_{QP} for the most abundant nuclei (those which contribute the most to the computation of the isospin transport ratio). The corresponding average excitation energy for each domain of $c_{E_{t12}}$ is also reported in the figure.

Concerning the ^{48}Ca + ^{40}Ca system (blue open triangles), we observe a behavior similar to the one reported in [24]: the higher the average excitation energy of the QP, the closer the final QP remnant is to the EAL (dashed horizontal line). Futhermore, we observe that the reduced chi-squared, χ^2, obtained from a linear fit to the ^{48}Ca + ^{40}Ca data (continuous line) increases with decreasing average excitation energy, showing more particularly that the correlation is not linear for the less dissipative collisions where $\langle E^*/A\rangle = 1.3$ MeV/nucleon.

Concerning the ^{40}Ca + ^{48}Ca system (red open dots), the interpretation is not straightforward, as a clear linearity of the correlation between $\langle\delta\rangle_{PLF}$ and δ_{QP} is not verified. We observe nonetheless a general evolution of the asymmetry to higher values for both the QP and the PLF with increasing average excitation energy, so that the values increasingly cross the EAL.

According to the aforementioned observations, we believe the reconstructed QP asymmetry to be more relevant in order to directly estimate the transport coefficients [10].

B. Isospin migration

As previously discussed, a possible indication of the isospin migration is a neutron enrichment in the neck region induced by a local density gradient in the portion of nuclear matter formed during the collision.

To study this phenomenon experimentally, we focus on the average neutron-to-proton ratio $\langle N/Z\rangle_{CP}$ of the clusters isotopically identified with INDRA and defined as

$$\langle N/Z\rangle_{CP} = \frac{\sum_\nu M_\nu \frac{N_\nu}{Z_\nu}}{\sum_\nu M_\nu},\qquad(8)$$

where M_ν, N_ν, and Z_ν are respectively the multiplicity, neutron number, and proton number of each cluster ν, where ν corresponds to ^{2,3}H, ^{3,4,6}He, ^{6,7,8,9}Li, or ^{7,9,10}Be isotopes (free protons and undetected neutrons are excluded). Thus, by construction, a neutron richness would be indicated by $\langle N/Z\rangle_{CP} > 1$.
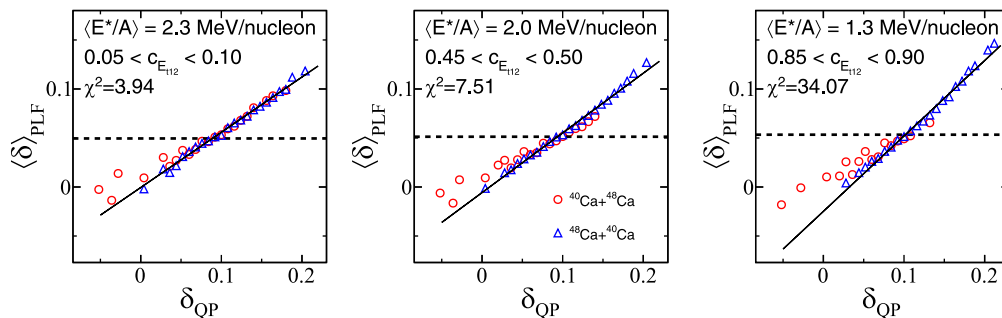

FIG. 5. Correlations between the asymmetry obtained from the QP remnant measured with VAMOS and the reconstructed QP for the mixed systems and different domains of $c_{E_{t12}}$, for the most abundant nuclei. Statistical error bars are smaller than the symbols. The continuous and dashed lines represents the linear fits and values predicted by the EAL for the ^{48}Ca + ^{40}Ca system, respectively.
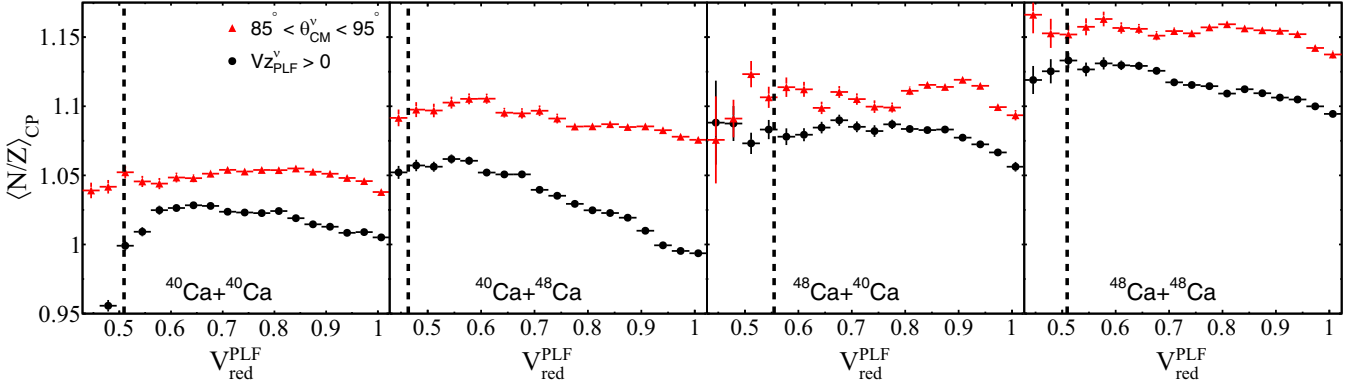
FIG. 6. Average $\langle N/Z \rangle_{CP}$ [see Eq. (8)] for each bin of PLF reduced velocity, for the clusters emitted forward with respect to the PLF (full circles) and in the angular region centered around the midrapidity (full triangles). Error bars, when larger than the symbols, represent the statistical error on the mean. Center-of-mass reduced velocity is represented with a dotted line.

In particular, we studied the clusters emitted (i) forward with respect to the PLF and (ii) in an angular region centered around the midrapidity of the reaction. The forward domain of the PLF, corresponding to clusters with a positive parallel velocity in the PLF reference frame ($Vz_{PLF}^{\nu} > 0$), is expected to be mostly populated by the decay emissions of the QP, minimizing contamination by the QT and neck (dynamical) emissions. The midrapidity domain, corresponding to an angular region centered around midrapidity in the reaction center of mass frame ($85° < \theta_{CM}^{\nu} < 95°$) is expected to be dominated by neck emissions [35].

The reduced velocity of the PLF, defined as $V_{red}^{PLF} = Vz^{PLF}/V^{proj}$, where Vz^{PLF} and V^{proj} are respectively the parallel velocity of the PLF and the projectile velocity in the laboratory, was chosen as a surrogate for the measure of the degree of dissipation of the collisions. It also presents the advantage of being independent of the $\langle N/Z \rangle_{CP}$ computed with the LCPs identified with INDRA, avoiding trivial bias due to autocorrelation with the event sorting. It should be noted that the results and conclusions presented hereafter can also be drawn using various N/Z ratios for complex particles described in the literature, such as the one defined in [27,36].

The results are presented in Fig. 6, where the average $\langle N/Z \rangle_{CP}$ is plotted as a function of V_{red}^{PLF}.

Concerning the forward emission region, we remark that the $\langle N/Z \rangle_{CP}$ tends to follow the hierarchy of the asymmetry δ observed in Fig. 3. This suggests that the measured N/Z ratio for complex particles can also be exploited as an alternative probe to evaluate the isospin transport ratio in peripheral collisions with the INDRA-VAMOS coupling. Concerning emissions at midrapidity, we observe higher $\langle N/Z \rangle_{CP}$ values compared to the forward domain, independently of the dissipation. This suggests a systematic neutron enrichment of the midrapidity region, which is dominated by the density drop at midrapidity rather than by the isotopic content of the colliding partners, in particular when they are symmetric [37]. Such observation can be interpreted as a consequence of isospin migration. Furthermore, free protons, most of which originate from prompt out-of-equilibrium emissions, are in fact excluded in the computation of $\langle N/Z \rangle_{CP}$. Finally, an overall smoother increase of $\langle N/Z \rangle_{CP}$ is observed with increasing

dissipation for the midrapidity region compared to the forward region.

In order to further investigate the individual contributions to the midrapidity region, we present in Fig. 7 the average multiplicities of the LCPs that contribute the most to the computation of $\langle N/Z \rangle_{CP}$, as a function of the reduced velocity of the PLF. For the sake of concision, the proton multiplicities are also represented here, but we remind that they are not included in Eq. (8).

As expected, the multiplicities increase with decreasing V_{red}^{PLF}, reflecting an increase of cluster production with increasing dissipation as more excitation energy is available. We observe that, for the protons and neutron-poor ^{3}He particles, the multiplicities mostly reflect the total (projectile and target) neutron content of the initial colliding system, leading to close distributions for the mixed ^{40}Ca + ^{48}Ca and ^{48}Ca + ^{40}Ca systems in the case of more dissipative collisions. We would like to highlight that this pattern is very different from the
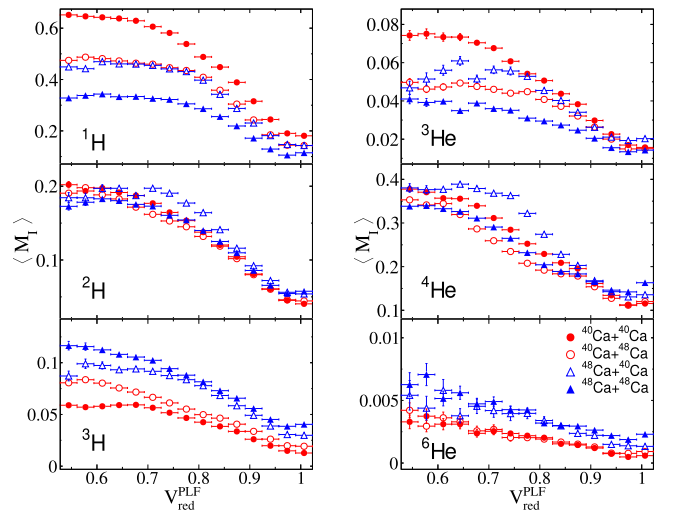

FIG. 7. Average LCP multiplicities detected in INDRA as a function of the QP remnant reduced velocity for the midrapidity domain (see text).

one obtained for the forward domain (see Fig. 8 from [18]), where a hierarchy related, first, to the neutron richness of the projectile and, to a lesser extent, of the target, is observed. Concerning the neutron-rich tritons and ^{6}He particles, we notice that the distributions mostly depend on the projectile neutron richness. Finally, in the case of the deuterons and ^{4}He particles, having the same N/Z, we observe that the multiplicities remain very close and depend much less on the system, similarly to the forward domain, with a noticeable difference for the ^{48}Ca + ^{40}Ca system. Surprisingly, we also remark that the absolute values are close for the symmetric systems independently of the centrality.

As a conclusion, the trends observed in Fig. 7 suggest that the behavior of $\langle N/Z \rangle_{CP}$, thus the neutron-enrichment of the midrapidity domain, is mainly driven by the $A = 3$ LCPs' isobars. Indeed, contrary to what we observe for the forward velocity domain, the ^{3}He and ^{3}H multiplicities mainly depend on the neutron richness of the total system or the projectile, respectively. Thus, for the symmetric system, the behavior is straightforward and independent of the dissipation as the neutron richness of the total system and the projectile act in phase, leading to higher values of $\langle N/Z \rangle_{CP}$ for the ^{48}Ca + ^{48}Ca reaction. For the asymmetric systems, the effect is more complex as the ^{3}He multiplicities tend to converge with increasing centrality, leading to values of $\langle N/Z \rangle_{CP} \simeq 1.1$ for both systems.

The above observations suggest that the experimental isotopic ratios reflect a neutron enrichment in the midrapidity velocity region. This can be interpreted as consequence of isospin migration, confirming that the density at midrapidity is lower than the saturation density ρ_0, resulting in the neutrons being attracted towards this zone. Also, similarly to the study given in [38] for heavier partners ^{136,124}Xe + ^{124,112}Sn reactions, we believe that comparisons of the triton and ^{3,6}He particles' production with filtered transport model calculations, more specifically for peripheral collisions, could lead to a better understanding of isospin dependence of the NEoS.

IV. CONCLUSION

In this work we investigated isospin transport phenomena in ^{40,48}Ca + ^{40,48}Ca reactions at 35 MeV/nucleon measured with the INDRA-VAMOS coupling.

By means of isospin transport ratios from both PLF and reconstructed QP, we have shown a clear evolution towards isospin equilibration with increasing dissipation of the collision, while a full N/Z equilibration condition is not reached, even for the most dissipative collisions measured. This evolution is even smoother for the reconstructed QP. In this respect, we have also explored quantitatively the correlation between the QP and PLF asymmetries and noticed that the linearity of the correlation disappears for the less dissipative collisions for the ^{48}Ca + ^{40}Ca system. We also observed that the higher the average excitation energy of the QP, the closer the final QP remnant is to the EAL.

Isospin migration was studied with the isotopic composition of light clusters ($Z \leqslant 4$) as the violence of the collision increases. An enhanced neutron enrichment of the midrapidity region (neck emissions) with respect to the forward-emitting region (QP emissions) is evidenced. This result is observed in the collisions between systems with the same N/Z asymmetry, thus clearly indicating that it is fully driven by isospin migration along the neck. The observed neutron enrichment in the neck seems to be dominated by $A = 3$ isobars.

The results presented in this work demonstrate the potential of the INDRA-VAMOS coupling to provide further constraints on the symmetry energy term in the NEoS. Comparisons of this dataset with dynamical and statistical model calculations are foreseen.

[1] J. M. Lattimer and M. Prakash, Phys. Rep. **621**, 127 (2016), Memorial Volume in Honor of Gerald E. Brown.

[2] M. B. Tsang, Y. Zhang, P. Danielewicz, M. Famiano, Z. Li, W. G. Lynch, and A. W. Steiner, Phys. Rev. Lett. **102**, 122701 (2009).

[3] H. Pais, F. Gulminelli, C. Providência, and G. Röpke, Phys. Rev. C **99**, 055806 (2019).

[4] A. Le Fèvre, Y. Leifels, W. Reisdorf, J. Aichelin, and C. Hartnack, Nucl. Phys. A **945**, 112 (2016).

[5] P. Russotto, S. Gannon, S. Kupny, P. Lasko, L. Acosta, M. Adamczyk, A. Al-Ajlan, M. Al-Garawi, S. Al-Homaidhi, F. Amorini *et al.*, Phys. Rev. C **94**, 034608 (2016).

[6] B. P. Abbott, R. Abbott, T. D. Abbott, F. Acernese, K. Ackley, C. Adams, T. Adams, P. Addesso, R. X. Adhikari, V. B. Adya *et al.*, Phys. Rev. Lett. **119**, 161101 (2017).

[7] M. C. Miller, F. K. Lamb, A. J. Dittmann, S. Bogdanov, Z. Arzoumanian, K. C. Gendreau, S. Guillot, A. K. Harding, W. C. G. Ho, J. M. Lattimer *et al.*, Astrophys. J. **887**, L24 (2019).

[8] S. Huth, P. T. H. Pang, I. Tews, T. Dietrich, A. Le Fèvre, A. Schwenk, W. Trautmann, K. Agarwal, M. Bulla, M. W. Coughlin *et al.*, Nature (London) **606**, 276 (2022).

[9] V. Baran, M. Colonna, and M. Di Toro, Nucl. Phys. A **730**, 329 (2004).

[10] V. Baran, M. Colonna, M. Di Toro, M. Zielinska-Pfabé, and H. H. Wolter, Phys. Rev. C **72**, 064620 (2005).

[11] E. Galichet, M. Colonna, B. Borderie, and M. F. Rivet, Phys. Rev. C **79**, 064615 (2009).

[12] M. B. Tsang, T. X. Liu, L. Shi, P. Danielewicz, C. K. Gelbke, X. D. Liu, W. G. Lynch, W. P. Tan, G. Verde, A. Wagner *et al.*, Phys. Rev. Lett. **92**, 062701 (2004).

[13] L.-W. Chen, C. M. Ko, and B.-A. Li, Phys. Rev. Lett. **94**, 032701 (2005).

[14] V. Baran, M. Colonna, V. Greco, and M. Di Toro, Phys. Rep. **410**, 335 (2005).

[15] R. Lionti, V. Baran, M. Colonna, and M. Di Toro, Phys. Lett. B **625**, 33 (2005).

[16] D. D. S. Coupland, W. G. Lynch, M. B. Tsang, P. Danielewicz, and Y. Zhang, Phys. Rev. C **84**, 054603 (2011).

[17] M. Colonna, V. Baran, and M. Di Toro, Eur. Phys. J. A **50**, 30 (2014).

[18] Q. Fable, A. Chbihi, M. Boisjoli, J. D. Frankland, A. Le Fèvre, N. Le Neindre, P. Marini, G. Verde, G. Ademard, L. Bardelli *et al.*, Phys. Rev. C **106**, 024605 (2022).

[19] J. Pouthas, B. Borderie, R. Dayras, E. Plagnol, M. F. Rivet, F. Saint-Laurent, J. C. Steckmeyer, G. Auger, C. O. Bacri, S. Barbey *et al.*, Nucl. Instrum. Methods Phys. Res., Sect. A **357**, 418 (1995).

[20] J. Pouthas, A. Bertaut, B. Borderie, P. Bourgault, B. Cahan, G. Carles, D. Charlet, D. Cussol, R. Dayras, M. Engrand *et al.*, Nucl. Instrum. Methods Phys. Res., Sect. A **369**, 222 (1996).

[21] S. Pullanhiotan, M. Rejmund, A. Navin, W. Mittig, and S. Bhattacharyya, Nucl. Instrum. Methods Phys. Res., Sect. A **593**, 343 (2008).

[22] F. Rami, Y. Leifels, B. de Schauenburg, A. Gobbi, B. Hong, J. P. Alard, A. Andronic, R. Averbeck, V. Barret, Z. Basrak *et al.*, Phys. Rev. Lett. **84**, 1120 (2000).

[23] A. Ono, Prog. Part. Nucl. Phys. **105**, 139 (2019).

[24] A. Camaiani, S. Piantelli, A. Ono, G. Casini, B. Borderie, R. Bougault, C. Ciampi, J. A. Dueñas, C. Frosin, J. D. Frankland *et al.*, Phys. Rev. C **102**, 044607 (2020).

[25] J. Łukasik, J. Benlliure, V. Métivier, E. Plagnol, B. Tamain, G. Auger, C. O. Bacri, E. Bisquer, B. Borderie, R. Bougault *et al.* (INDRA Collaboration), Phys. Rev. C **55**, 1906 (1997).

[26] E. Plagnol, J. Łukasik, G. Auger, C. O. Bacri, N. Bellaize, F. Bocage, B. Borderie, R. Bougault, R. Brou, P. Buchet *et al.*, Phys. Rev. C **61**, 014606 (1999).

[27] G. Ademard, B. Borderie, A. Chbihi, O. Lopez, P. Napolitani, M. F. Rivet, M. Boisjoli, E. Bonnet, R. Bougault *et al.* (INDRA Collaboration), Eur. Phys. J. A **50**, 33 (2014).

[28] J. D. Frankland, D. Gruyer, E. Bonnet, B. Borderie, R. Bougault, A. Chbihi, J. E. Ducret, D. Durand, Q. Fable, M. Henri *et al.*, Phys. Rev. C **104**, 034609 (2021).

[29] C. Ciampi, S. Piantelli, G. Casini, G. Pasquali, J. Quicray, L. Baldesi, S. Barlini, B. Borderie, R. Bougault, A. Camaiani *et al.*, Phys. Rev. C **106**, 024603 (2022).

[30] R. J. Charity, Phys. Rev. C **58**, 1073 (1998).

[31] P. Napolitani, K.-H. Schmidt, L. Tassan-Got, P. Armbruster, T. Enqvist, A. Heinz, V. Henzl, D. Henzlova, A. Kelić, R. Pleskač, M. V. Ricciardi, C. Schmitt, O. Yordanov, L. Audouin, M. Bernas, A. Lafriaskh, F. Rejmund, C. Stephan, J. Benlliure, E. Casarejos, M. FernandezOrdonez, J. Pereira, A. Boudard, B. Fernandez, S. Leray, C. Villagrasa, and C. Volant, Phys. Rev. C **76**, 064609 (2007).

[32] D. Henzlova, K.-H. Schmidt, M. V. Ricciardi, A. Kelić, V. Henzl, P. Napolitani, L. Audouin, J. Benlliure, A. Boudard, E. Casarejos *et al.*, Phys. Rev. C **78**, 044616 (2008).

[33] Z. Y. Sun, M. B. Tsang, W. G. Lynch, G. Verde, F. Amorini, L. Andronenko, M. Andronenko, G. Cardella, M. Chatterje, P. Danielewicz *et al.*, Phys. Rev. C **82**, 051603(R) (2010).

[34] L. W. May, A. Wakhle, A. B. McIntosh, Z. Kohley, S. Behling, A. Bonasera, G. Bonasera, P. Cammarata, K. Hagel, L. Heilborn *et al.*, Phys. Rev. C **98**, 044602 (2018).

[35] S. Piantelli, L. Bidini, G. Poggi, M. Bini, G. Casini, P. R. Maurenzig, A. Olmi, G. Pasquali, A. A. Stefanini, and N. Taccetti, Phys. Rev. Lett. **88**, 052701 (2002).

[36] E. Galichet, M. F. Rivet, B. Borderie, M. Colonna, R. Bougault, A. Chbihi, R. Dayras, D. Durand, J. D. Frankland, D. C. R. Guinet *et al.*, Phys. Rev. C **79**, 064614 (2009).

[37] D. Thériault, J. Gauthier, F. Grenier, F. Moisan, C. St-Pierre, R. Roy, B. Davin, S. Hudan, T. Paduszynski, R. T. de Souza, E. Bell, J. Garey, J. Iglio, A. L. Keksis, S. Parketon, C. Richers, D. V. Shetty, S. N. Soisson, G. A. Souliotis, B. C. Stein, and S. J. Yennello, Phys. Rev. C **74**, 051602(R) (2006).

[38] R. Bougault, E. Bonnet, B. Borderie, A. Chbihi, D. Dell'Aquila, Q. Fable, L. Francalanza, J. D. Frankland, E. Galichet, D. Gruyer *et al.*, Phys. Rev. C **97**, 024612 (2018).